PHYSICAL REVIEW B **68**, 125313 (2003)

Relaxation oscillations and dynamical enhancement of the breakdown hysteresis in quantum Hall systems with Corbino geometry

N. G. Kalugin,[1,*] B. E. Sağol,[1] A. Buß,[1] A. Hirsch,[1] C. Stellmach,[1] G. Hein,[2] and G. Nachtwei[1]
[1]*Institut für Technische Physik, TU-Braunschweig, Mendelssohnstr. 2, D-38106 Braunschweig, Germany*
[2]*Physikalisch-Technische Bundesanstalt, Bundesallee 100, D-38116 Braunschweig, Germany*

(Received 11 March 2003; published 16 September 2003)

Using the bistability of quantum Hall systems in the hysteresis region of the breakdown, we realized a simple relaxation oscillator based on a quantum Hall device with Corbino geometry. Investigations of the performance of such an oscillator revealed the increase of the hysteresis of the current-voltage curve of the device in comparison with the value of hysteresis at dc voltages. By direct measurements of the hysteresis of the current-voltage curve at different frequencies, we have found that a dramatic increase of the breakdown hysteresis happens already at low (Hz-range) frequencies. We explain the observed dynamical enhancement of the breakdown hysteresis using an electron heating model and the assumption of a decreasing background (delocalization-related) component of the conductivity with increasing frequency.

DOI: 10.1103/PhysRevB.68.125313 PACS number(s): 73.43.−f, 73.50.Fq, 73.50.Mx

I. INTRODUCTION

The bistability of the current-voltage ($I-V$) characteristics of electronic devices is widely in use for the generation of anharmonic oscillations. Various nonlinear bistable electronic devices have been used for the generation of electrical anharmonic oscillations so far, starting from the use of discharge tubes by Van der Pol and Van der Mark in 1927,[1] and ending by today's use of high-frequency resonant tunnel diodes[2] in the modern communication, data processing and optoelectronic systems. The studies of bistable systems are interesting not only from an applicative point of view, but also for a basic understanding of the nature of the underlying nonlinear phenomena.[3]

In this work we report on results of using the bistable behavior of devices, showing the quantum Hall effect[4] (QHE), near the QHE breakdown,[5] for the generation of anharmonic oscillations. Here, the bistability manifests itself in a hysteresis[6,7] of the current-voltage characteristics for the switching between a resistive and a nondissipative [quantum Hall (QH)] state. Our investigations of the working regimes of the relaxation oscillator on the basis of a QH device with a Corbino geometry, revealed not only the limiting points of such an oscillator, but also opened the way to investigate in more detail the mechanisms of the appearance and change of QHE breakdown hysteresis with the frequency. In particular, we have found a *dramatic increase of hysteresis* with increasing frequency *in the region of low (some Hz) frequencies*. We have found an explanation for this phenomenon, using an electron heating model[5,8] and the assumption of a suppression of the delocalization-related electron conductivity with increasing frequency. The reduction of the background conductivity corresponds to a shrinking of the localization length.[9–11] Therefore, our results reveal that near the QHE breakdown the localization length in QH systems with a Corbino geometry [in the low frequency (Hz) range] decreases with increasing frequency.

This paper is organized in the following way: in Sec. II we describe the properties of experimental samples. In Sec. III we give a detailed description of the observed features of the QH Corbino relaxation oscillator. Section IV is focused on direct measurements of the frequency dependence of the breakdown hysteresis in QH Corbino devices. In Sec. V we discuss our results on the basis of an electron heating model. The Appendix describes in detail the electron heating model, as used for explanation of experimental results.

II. EXPERIMENTAL SAMPLES

We have patterned circular Corbino devices on a GaAs/GaAlAs heterostructure wafer with an electron density of $n_s = 2.9\times10^{11}$ cm^{-2} and a Hall mobility of $\mu_H = 1\times10^5$ cm^2/V s. Samples of two geometries were investigated: both samples had the same radius of inner contact 100 μm, but different radii of outer contact 300 μm (sample A) and 200 μm (sample B).

III. RELAXATION OSCILLATIONS IN QUANTUM HALL CORBINO DEVICES

A particularly suitable device to set up an oscillator on the basis of a quantum Hall system is the Corbino device. This is because such a device shows an almost ideal insulating behavior in the QH regime until a certain, critical value V_{max} of the source-drain voltage V_{SD} (Ref. 12). At V_{max}, a sudden onset of the source-drain current I_{SD} occurs. A subsequent reduction of V_{SD} leads to a sudden interruption of I_{SD} at another critical voltage V_{min} ($V_{min} < V_{max}$). In the hysteresis region $V_{min} < V_{SD} < V_{max}$, the QH device behaves bistable. If a resistance is connected in series and a capacitor is used as an accumulating device in parallel to the QH device, the bistable switching leads to a subsequent charging and discharging of the capacitor, detectable as relaxation oscillations.

In the real experiment, the cables connecting different parts of the oscillator already work effectively as a capacitor. The cable capacitance is one of the crucial limits of the maximal frequency which can be reached with the oscillator.

Oscillators with different circuitry parameters were based

 ©2003 The American Physical Society

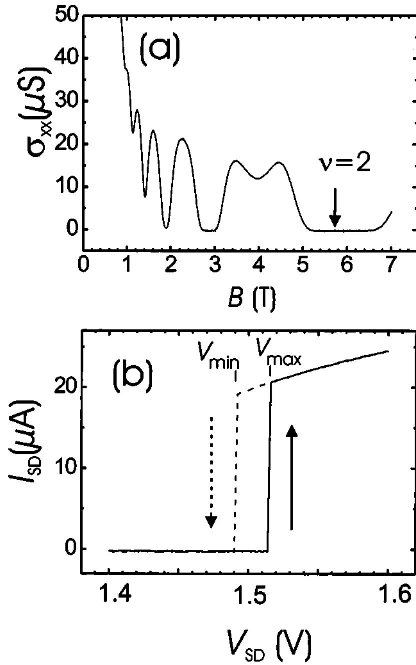

FIG. 1. (a) Shubnikov–de Haas oscillations [constant voltage (dc) measurement of $\sigma_{xx}(B)$ at $V_{SD}=100$ mV] of the QH Corbino device (sample A, $R_{CB}=76$ kΩ). (b) dc current-voltage characteristics of the Corbino sample at $B=5.7$ T (second QH plateau). $T=1.5$ K.

on sample A. The sample properties n_s and μ_H were deduced from Shubnikov–de Haas oscillations [Fig. 1(a)] and the QH breakdown properties from the $I-V$ characteristics [source-drain current I_{SD} versus source drain voltage V_{SD}; see Fig. 1(b)].

From Fig. 1(b), the hysteresis of the QH-breakdown with respect to the critical source-drain-voltage is clearly visible. The corresponding bistable region of the $I-V$ curve is exploited for our oscillator. The scheme of the oscillator circuit and the function principle are sketched in Figs. 2(a) and 2(b) (Ref. 13). The total capacitance (capacitor C_T) is charged via the serial resistor R_V, until the breakdown voltage V_{max} (upsweep) is reached. During this process, the Corbino device is

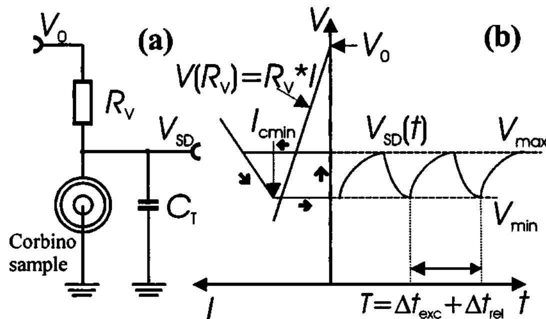

FIG. 2. (a) Scheme of the oscillator circuit. R_V is the serial resistance, C_T is the total capacitance of the circuit. (b) Function principle of the oscillator. For an appropriate choice of R_V and the driving voltage V_0, oscillations of the voltage V_{SD} at the Corbino device occur between the dynamical hysteresis limits V_{min} and V_{max}.

insulating and acts like an open switch. The voltage V_{max} closes the switch, and C_T starts to discharge via the Corbino device, which now has a finite resistance R_{CB}. This process endures until the voltage falls to V_{min}, at which the Corbino device becomes insulating again. Thus the oscillation amplitude ΔV is determined by the hysteresis, $\Delta V=V_{max}-V_{min}$.

From Fig. 2(b), it can be seen that there is a certain range for the choice of the driving voltage V_0 and the serial resistor R_V to keep the oscillator inside the working regime: (a) The current through R_V for the Corbino device being at V_{min} must not exceed the limit $I_c^{min}=V_{min}/R_{CB}$ (for $V_0-V_{min}\geqslant R_V I_c^{min}$, a stable solution exists on the resistive branch of the $I-V$ curve of the QH device, corresponding to a stationary state without oscillations). (b) The driving voltage must be $V_0>V_{max}$.

From conditions (a) and (b), it can be concluded that the lower limit for the serial resistance value is $R_V>\Delta V/I_c^{min}$. Once R_V is chosen, the choice determines the operational range for the driving voltage V_0 according to condition (a):

$$\frac{V_0-V_{min}}{R_V}<\frac{V_{min}}{R_{CB}}, \quad \text{thus} \quad V_{max}<V_0<V_{min}\frac{R_{CB}+R_V}{R_{CB}}. \tag{1}$$

The time constants τ_{exc} and τ_{rel}, as well as the voltage V_{SD} at the Corbino device, for the charging and discharging processes can be determined from the solutions of Kirchhoff's equations with an open switch and R_{CB}, respectively. This yields (akin to the results for relaxation oscillators based on tunnel diode circuits[14]) exponential time dependences:

$$V_{SD}(t)=V_0-(V_0-V_{min})\exp\left\{-\frac{t}{\tau_{exc}}\right\} \quad \text{with} \quad \tau_{exc}=R_V C_T. \tag{2}$$

for the charging, and

$$V_{SD}(t)=V_{max}\exp\left\{-\frac{t}{\tau_{rel}}\right\} + V_0\frac{R_{CB}}{R_{CB}+R_V}\left(1-\exp\left\{-\frac{t}{\tau_{rel}}\right\}\right)$$

with

$$\tau_{rel}=\frac{R_{CB}R_V}{R_{CB}+R_V}C_T. \tag{3}$$

for the discharging, where R_V and R_{CB} act as parallel resistors. The oscillation period $T=\Delta t_{exc}+\Delta t_{rel}$ is not only determined by τ_{exc} and τ_{rel}, but also by the hysteresis limits V_{max} and V_{min}, and by the driving voltage V_0 with

$$\Delta t_{exc}=\tau_{exc}\ln\left(\frac{V_0-V_{min}}{V_0-V_{max}}\right), \tag{4a}$$

$$\Delta t_{rel}=\tau_{rel}\ln\left(\frac{V_{max}-\Theta V_0}{V_{min}-\Theta V_0}\right), \tag{4b}$$

with

$$\Theta=\frac{R_{CB}}{R_{CB}+R_V}.$$

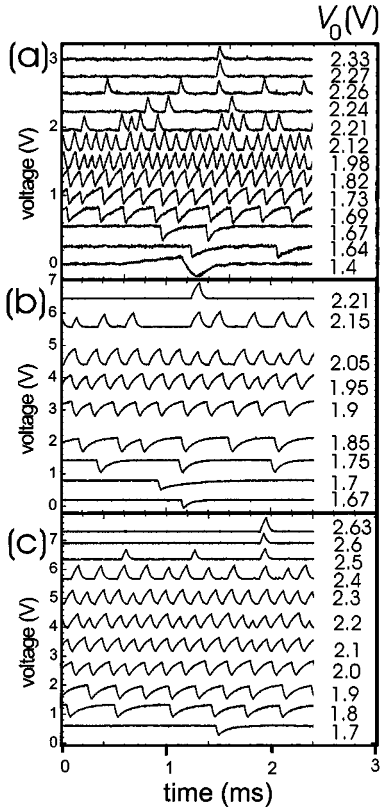

FIG. 3. Relaxation oscillations of the Corbino oscillator (sample A), $T=1.5$ K, $B=5.7$ T, second QH plateau, for the following. (a) Circuit case #1: $R_{\mathrm{CB}}=76\ \mathrm{k}\Omega$, $R_V=46\ \mathrm{k}\Omega$, $C_T=2.1$ nF, at different driving voltages V_0 (curves shifted for clarity). The oscillator operates at V_0 between 1.65 and 2.25 V. Whereas the oscillation amplitude is almost constant within this range, the frequency changes and has a maximum at $V_0\approx 2$ V. (b) Circuit case #2: $R_{\mathrm{CB}}=90\ \mathrm{k}\Omega$, $R_V=46\ \mathrm{k}\Omega$, $C_T=1.5$ nF. (c) Circuit case #3: $R_{\mathrm{CB}}=90\ \mathrm{k}\Omega$, $R_V=68\ \mathrm{k}\Omega$, $C_T=1.5$ nF, at different driving voltages V_0 (curves shifted for clarity).

With an increasing driving voltage V_0, the charging time Δt_{exc} decreases and the discharging time Δt_{rel} increases [for V_0 in the operation interval as given in Eq. (1)]. The oscillation frequency f as a function of V_0 has a maximum value at

$$V_0(f_{\max})=\frac{V_{\min}V_{\max}}{V_{\min}+V_{\max}}\left(2+\frac{R_V}{R_{\mathrm{CB}}}\right), \tag{5}$$

which does not depend on the capacitance C_T.

At V_0 ($f_{\max}$), the oscillator frequency can exceed the value $f=(\tau_{\mathrm{exc}}+\tau_{\mathrm{rel}})^{-1}$ considerably. The maximum frequency of the oscillator shows a complicated dependence on $V_{\max}$, $V_{\min}$, C_T, R_{CB}, and, in particular, on the value of R_V. This is discussed in detail below [Fig. 5(b)].

Figure 3 shows a set of measured oscillation curves $V_{\mathrm{SD}}(t)$ for various values of the driving voltage V_0 for different circuit parameters. For Fig. 3(a), the resistance of the Corbino sample A was found to be $R_{\mathrm{CB}}=76\ \mathrm{k}\Omega$, and the hysteresis size (region of voltages where the sample was bistable) from dc measurements was found equal to 25 mV.

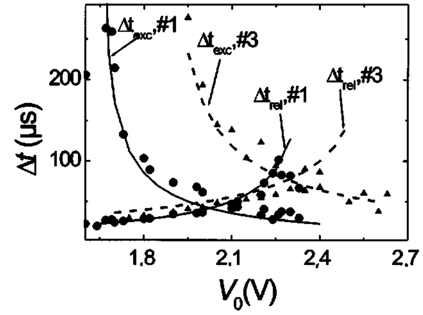

FIG. 4. Measured charging times Δt_{exc} and discharging times Δt_{rel} of the QH Corbino oscillator on the basis of sample A, $T=1.5$ K, $B=5.7$ T, and the second QH plateau. (a) For case #1: $R_{\mathrm{CB}}=76\ \mathrm{k}\Omega$, $R_V=46\ \mathrm{k}\Omega$, $C_T=2.1$ nF, as a function of the driving voltage V_0, in comparison to the calculated values (solid line, full dots) with the parameters $\tau_{\mathrm{exc}}=96\ \mu$s, $\tau_{\mathrm{rel}}=60\ \mu$s, $V_{\min}=1.46$ V, $V_{\max}=1.66$ V, dynamical hysteresis size $\Delta V=0.2$ V. (b) For case #3: $R_{\mathrm{CB}}=90\ \mathrm{k}\Omega$, $R_V=68\ \mathrm{k}\Omega$, $C_T=1.5$ nF as a function of the driving voltage V_0, in comparison to the calculated values (dashed line, triangles) with the parameters $\tau_{\mathrm{exc}}=102\ \mu$s, $\tau_{\mathrm{rel}}=58\ \mu$s, $V_{\min}=1.42$ V, $V_{\max}=1.9$ V, and dynamical hysteresis size $\Delta V=0.46$ V.

To ensure the working regime of the oscillator, we have chosen a serial resistor $R_V=46\ \mathrm{k}\Omega$ of comparable size with the dissipative Corbino resistance. From the $I-V$ curve [Figs. 1(b)] and Eq. (1), this would yield an operation interval for V_0 from 1.52 to 2.39 V. But, as seen from Fig. 3(a), the oscillator works within about 1.65 V$<V_0<$2.25 V, an interval which is distinctively narrower than the one deduced from the dc-measured hysteresis of the $I-V$ curve. In turn, the amplitude is larger than ΔV taken from Fig. 1(b). Both discrepancies can be resolved simultaneously taking into account a wider dynamical hysteresis at the oscillator frequencies of some kHz in comparison to the quasistationary one. As we see, the measured oscillation amplitude is a direct measure of the dynamical hysteresis of the QHE breakdown at the oscillation frequency. The amplitude of the oscillations remained almost unchanged with V_0 in the working regime (180–250 mV, close to the operation limits of the oscillator the amplitudes tend to vary).

The measured charging and discharging times show a pronounced V_0 dependence, which we used to estimate the total capacitance C_T of the circuit. To reach higher frequencies, no separate capacitor was attached, so that C_T is dominated by the capacitance of cables and connectors (for C_T, the capacitances of the Corbino device (<0.1 pF) and of the input of the oscilloscope (20 pF) can be neglected). From the measured values of Δt_{exc} and Δt_{rel} as a function of V_0, the best fit applying Eq. (4) was obtained with $C_T=2.1$ nF. (For simplicity and for a better orientation in the curves of the figures, we shall call this set of parameters case #1: $R_{\mathrm{CB}}=76\ \mathrm{k}\Omega$, $R_V=46\ \mathrm{k}\Omega$, $C_T=2.1$ nF). Figure 4 presents the corresponding data in comparison to the calculated dependences. The measured dependences of Δt_{exc} and Δt_{rel} on V_0 are reproduced quite well. The calculations yield a maximum oscillation frequency of 11.9 kHz at $V_0=2.02$ V, which is in reasonable agreement with the experimental value of $f_{\max}=11.2$ kHz at $V_0=2.1$ V (also see Fig. 5).

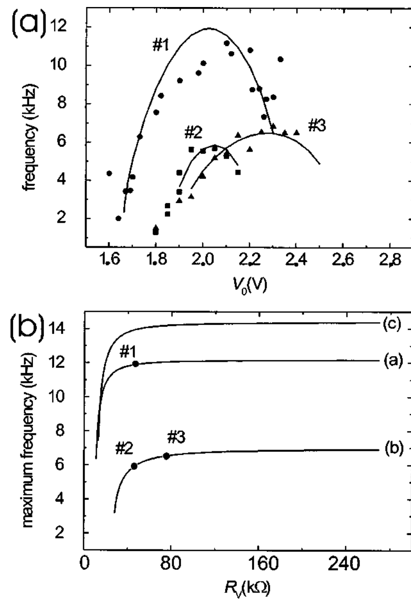

FIG. 5. (a) Frequency of relaxation oscillations as the function of driving voltage V_0 for an oscillator on the basis of sample A with the following circuit parameters: case #1 [full dots; corresponds to Fig. 3(a)], $R_{\mathrm{CB}}=76\ \mathrm{k}\Omega$ (amplitude of dynamical hysteresis $\Delta V=0.2$ V), $R_V=46\ \mathrm{k}\Omega$, $C_T=2.1$ nF; case #2 [squares; see Fig. 3(b)], $R_{\mathrm{CB}}=90\ \mathrm{k}\Omega$ ($\Delta V=0.46$ V), $R_V=46\ \mathrm{k}\Omega$, $C_T=1.5$ nF; case #3, $R_{\mathrm{CB}}=90\ \mathrm{k}\Omega$ ($\Delta V=0.46$ V), $R_V=68\ \mathrm{k}\Omega$, $C_T=1.5$ nF [triangles; also see Fig. 3(c)]; symbols – measured values; solid lines – model. (b) Results of calculations of the maximal oscillation frequency [according to Eq. (4)] vs R_V for sample A with (a) $R_{\mathrm{CB}}=76\ \mathrm{k}\Omega$, $C_T=2.1$ nF, $V_{\min}=1.46$ V, $V_{\max}=1.66$ V ($\Delta V=0.2$ V), (b) $R_{\mathrm{CB}}=90\ \mathrm{k}\Omega$, $C_T=1.5$ nF, $V_{\min}=1.42$ V, $V_{\max}=1.9$ V ($\Delta V=0.46$ V), (c) $R_{\mathrm{CB}}=76\ \mathrm{k}\Omega$, $C_T=1.5$ nF, $V_{\min}=1.46$ V, $V_{\max}=1.66$ V ($\Delta V=0.2$ V). The points corresponding to the cases of circuits #'s 1, 2, and 3 are indicated. (b) clearly explains the experimental observations of (a).

Figures 3(b) and 3(c) demonstrate the shape of oscillations for an oscillator with changed circuit parameters. For both Figs. 3(b) and 3(c), as a result of a repeated cooling cycle of the sample from room temperature upto the working temperature at 1.5 K, the resistance of Corbino device (the same sample A) in a resistive state was found this time equal to $R_{\mathrm{CB}}=90\ \mathrm{k}\Omega$, the dc hysteresis size in this case was 20 mV. In order to decrease the capacitance of the circuit, we used shorter connection cables, resulting in a reduced cable capacitance of $C_T=1.5$ nF according to evaluations of experimental data (see Fig. 4). We also changed the serial resistor, in Fig. 3(b) $R_V=46\ \mathrm{k}\Omega$ (case #2), in Fig. 3(c) $R_V=90\ \mathrm{k}\Omega$ (case #3). According to the changed serial resistance R_v and the higher value of the dynamical hysteresis ($\Delta V=0.46$ V), the working region of the oscillator (region of V_0) shifts towards higher values (compare case #'s 1 and 3 in Fig. 4), and the frequencies of oscillations increase [compare the curves corresponding to case #'s 2 and 3 in Fig. 5(a)]. The reduction of a (cable) capacitance C_T should also lead to the increase of oscillation frequencies due to a decrease of τ_{exc} and τ_{rel}, [see Eqs. (2), (3), and (4)].

However, not only the serial resistance and the circuit capacitance are important for the frequency of relaxation oscillations. In our experiments we have reached the highest frequency of oscillations for the case, when C_T was not yet reduced, but the Corbino device itself had a lower R_{CB} and smaller amplitude of dynamical hysteresis $\Delta V-76\ \mathrm{k}\Omega$ and 0.2 V accordingly [see Fig. 5(a), compare point #1 with point #'s 2 and 3]. The observed behavior is well explainable by Fig. 5(b), which demonstrates the results of oscillator frequency calculations according to Eq. (4) for different R_v, C_T, R_{CB}, and for different amplitudes of the hysteresis. In Fig. 5(b) we clearly see, that if we keep the values constant for R_v and R_{CB}, and the amplitude of the hysteresis, the decrease of C_T leads to an increase of the oscillation frequency [compare curves (a) and (c)]. Surprisingly, the increase of R_V at constant C_T and R_{CB} also leads to an increase of the frequency until a saturation behavior is reached. It is clearly visible that the change of R_{CB} and the amplitude of the hysteresis influence the frequency dramatically: the case of a smaller hysteresis (smaller R_{CB}) corresponds to higher oscillation frequencies. Thus, higher frequencies can be realized only by a simultaneous reduction of the oscillation amplitude. It is worth to note that the model calculations agree excellently with the experimentally observed values of the frequencies (see Fig. 5(b), point #'s 1, 2, and 3).

There is one important detail in all of the numerical calculations which has a significant importance and will be discussed in detail in Sec. V and the Appendix of this paper: in all of our calculations [Figs. 4 and 5(b)], when we needed a description of the changes of the hysteresis amplitude, we had the best fit when we changed mainly the value $V_{\max}$, whereas changing $V_{\min}$ was found to be much less significant.

The physical limits of the oscillation frequency are given by the switching times of the Corbino device, which we have found to be rather short (a few nanoseconds in low-mobility samples[12]). With this, upper frequencies in the GHz range are potentially accessible. Of course, there are simpler solutions to generate GHz oscillations like, e.g., resonant tunnelling devices.[2] However, the oscillator as described above provides additional insight into the dynamical properties of the breakdown of the QHE (dynamical hysteresis). To summarize the results of this part, we can state the following.

(i) We realized the relaxation oscillator on the basis of a bistable QH Corbino device.

(ii) the main result in the performance of this oscillator is that the amplitude of the oscillations is much larger than one can expect from dc measurements of the hysteresis. This means that the dynamical hysteresis is larger than the dc one.

(iii) Our description, based on Kirchhoff's equations, explains all the behavior of the QH Corbino relaxation oscillator very well, if we take into account an enlarged dynamical hysteresis. The growth of this hysteresis is due to an increase of $V_{\max}$ at an almost unchanged $V_{\min}$.

IV. FREQUENCY DEPENDENCE OF BREAKDOWN HYSTERESIS IN QUANTUM HALL CORBINO SYSTEMS

The increase of the QH breakdown hysteresis, as observed in the Corbino QH device working in the core of a

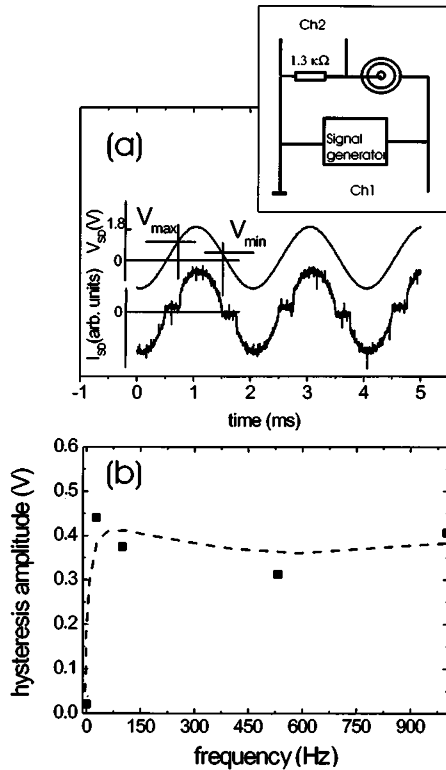

FIG. 6. (a) An example of oscilloscope traces of the voltage [sinusoidal signal, amplitude 1.8 V, frequency 500 Hz (top trace)] applied to the Corbino device, and of the corresponding current via sample *A* (the sample demonstrated a dc hysteresis amplitude of 25 mV, $R_{CB}=90$ kΩ, $B=5.7$ T, second QH plateau, $T=1.5$ K) (bottom trace). The points of switching, corresponding to voltages V_{max} and V_{min}, are clearly visible. Inset: the scheme for measurements of the dynamical hysteresis of a QH Corbino device. (b) The frequency dependence of the amplitude of the QH breakdown hysteresis ΔV of the sample *A*. We observe a dramatic (approximately 16 times) increase of the hysteresis at low frequencies.

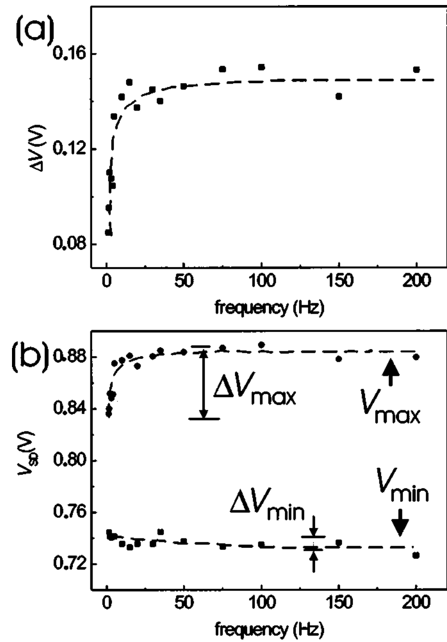

FIG. 7. (a) The frequency dependence of the amplitude of the QH breakdown hysteresis of sample *B*, $B=5.85$ T; second QH plateau, $T=1.5$ K. (b) The frequency dependence of the limits of the hysteresis curve, V_{min} and V_{max}, for sample *B*. Going from dc to higher frequencies, at low frequencies we see the growth of V_{max}, and a less pronounced change of V_{min}.

relaxation oscillator at frequencies of about 1–10 kHz, inspired us to direct measurements of the hysteresis parameters, and to do this in a wider range of frequencies. The measurements of this type were done using the scheme shown in the inset of Fig. 6(a). The voltage of the sinusoidal waveform, applied to sample *A* (the sample on which the oscillator was realized, with radii of the inner and outer contacts of 100 and 300 μm, accordingly) was monitored by an oscilloscope connected to channel 1 of the scheme; the current carried through the Corbino device was monitored via channel 2. The traces of the applied voltage, and of the current via the Corbino device, are shown in Fig. 6(a). As seen in Fig. 6(a) the "switching" of the Corbino device between the QHE-related insulator state at low voltages, and the resistive state at the supercritical voltages, is clearly distinguishable. This allowed us to measure directly the amplitude of an ac hysteresis $\Delta V=V_{max}-V_{min}$ for different frequencies. The result is shown in Fig. 6(b). As one can see in Fig. 6(b), we observed a *drastic increase of the hysteresis* at low frequencies (from 25 mV at dc to 0.4 V at 27 Hz) and a saturation at higher frequencies (0.3–0.4 V for *f* from 100 Hz to 1 kHz). At higher frequencies the amplitude of the dynamical hysteresis of sample *A*, as we see in Fig. 6(b), was found in complete accordance with the measurements as described above at the relaxation oscillator in circuitry case #1 [measurements of Figs. 3(a) and 6 were done in one cooling cycle of sample *A*).

We have performed more detailed measurements of the frequency dependence of the breakdown hysteresis, using sample *B* (with radii of inner and outer contacts of 100 and 200 μm, accordingly; the size of a dc hysteresis is approximately 100 mV; $R_{CB}=41$ kΩ in the resistive state). The results of measurements, similar to those described above with sample *A* (see Fig. 6), are presented in Fig. 7. As we see in Fig. 7(a), at low frequencies we again observed the typical growth of the hysteresis amplitude in the region between 0 and 20 Hz, and the saturation of the hysteresis at higher frequencies (with sample *B* we have observed a relative stability of the saturated value of the hysteresis up to 100 kHz). The experiment shows that this growth of the hysteresis is mainly the result of a growth of V_{max} with increasing frequency; at the same time the changes of V_{min} are much less pronounced. So, we see [Fig. 7(b)] an experimental confirmation of the change of V_{max}, and of the relative stability of V_{min} versus frequency, as earlier found from calculations using appropriate fit parameters for the observed relaxation oscillations (for a detailed discussion, see the Appendix).

As soon as it was found that the major changes in the hysteresis happen at low frequencies, the measurements at ultralow frequencies were done in order to complete the picture. Figure 8 shows the results of quasi-dc measurements of the *I*-*V* characteristic of the sample *B*, which have been done with different voltage sweep rates (in Fig. 8 the comments on

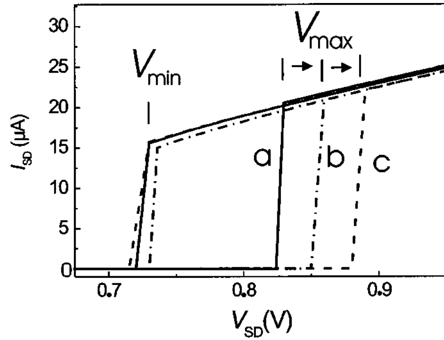

FIG. 8. The quasi-dc $I-V$ curves of a QH Corbino device (sample B, $B=5.85$ T; second QH plateau, $T=1.5$ K) at different voltage sweep rates. Corresponding effective frequencies of applied voltage are, accordingly 0.0065 Hz [(a), solid line] 0.029 Hz [(b), dash-dotted line], and 0.0333 Hz [(c), dashed line]. The increase of QH breakdown hysteresis, caused by the growth of V_{max} at a much less changed V_{min}, is clearly visible already at such a low frequencies.

the curves are made in terms of corresponding effective frequencies). We clearly see that even at such low frequencies there is a change of the hysteresis. We directly observe the evident growth of the hysteresis amplitude because of the growth of V_{max}, while V_{min} changes only slightly (Fig. 8).

V. DISCUSSION

A common explanation for the observed hysteresis of the current-voltage characteristics of QH devices at the breakdown of the quantum Hall effect can be derived from the electron heating model.[5,8] It is known[5,8] that the hysteresis arises from the metastability of the balance between electrical energy fed to the system per time and square unit (heating, "gain" of energy of electrons) $p_{gain}=\sigma_{xx}E_r^2$ (σ_{xx} is the longitudinal conductivity of the QH system, E_r is the radial electric field in the Corbino device), and the energy loss rate $p_{loss}=\varepsilon(T_{el})$-$\varepsilon(T_L)/\tau_{relax}$ (where T_{el} is the electron temperature, T_L is the lattice temperature, ε is the electron energy, τ_{relax} is the energy relaxation time, and k_B is the Boltzmann constant). The balance means $p_{gain}=p_{loss}$. The important point of the model (see the Appendix) is taking into account the different components of conductivity:

$$\sigma_{xx}(T_{el})=\sigma_0 \exp\{-\Delta/k_B T_{el}\}+\sigma_{BG},$$

where the first term describes the thermal activation of electron transitions between Landau levels (the activation gap is $\Delta=\hbar\omega_c/2$ (at even integer filling factors), where $\hbar\omega_c$ is cyclotron energy), and the second term σ_{BG} is a background conductivity corresponding to tunneling-related transport, caused by thermally assisted and (or) electric-field-assisted delocalization of electrons (also see Refs. 11 and 15). The model (for more details see the Appendix) allows us to describe the appearance and changes of the hysteresis in dependence on T_{el} versus the source-drain voltage V_{SD}, and, therefore, in I_{SD}-V_{SD} characteristics. The electron temperature T_{el} as a function of the source-drain voltage V_{SD} yields an S-shaped dependence (see the Appendix). Since σ_{xx} is a monotonous function of T_{el}, this corresponds to an S-shaped current-voltage characteristics.[5,8] The hysteresis is confined between two limiting values of V_{SD}, V_{max}, and V_{min}, and, accordingly, V_{max} corresponds to lower electron temperatures and V_{min} to higher electron temperatures.

Both values V_{max} and V_{min} (see the Appendix) depend on many parameters, but most essentially on the temperature dependence of $\sigma_{xx}(T_{el})$. The background, delocalization-related contribution to the conductivity, σ_{BG}, is of crucial influence on the breakdown voltage V_{max}. If a purely activated behavior of $\sigma_{xx}(T)$ is assumed, then the model also yields a hysteresis of I-V characteristic, but the values for V_{max} become unrealistically high. To obtain values of V_{max} closer to the experiment, additional transport mechanisms leading to finite values of σ_{BG} have to be assumed.

The value of V_{min}, which marks the lower limit of the hysteresis at higher electron temperatures, is nearly unaffected by the choice of σ_{BG}. This is due to the dominance of phonon-related scattering and activated transport at higher electron temperatures, as is relevant for V_{min}. For a determination of V_{min}, the activated conduction provides the dominating contribution. In turn, V_{max} depends distincty on σ_{BG}. With an increase of σ_{BG}, V_{max} exhibits a pronounced decrease up to the complete disappearance of the hysteresis at $\sigma_{BG}=1.3\times10^{-7}$ S$=1.7\times10^{-3}\sigma_{xy}$ for sample A (see the Appendix). This is due to the dominance of the additional contribution of σ_{BG} to the conductivity at lower electron temperatures, at which the activated conductivity is negligible.

As we see, by adjusting the value of σ_{BG}, one can directly interpret the observed frequency dependence of the hysteresis, obtained from investigations of the relaxation oscillator, as well as from direct measurements of the hysteresis parameters (see the sections above). The enhancement of the hysteresis with increasing frequency due to the increase of V_{max} (and the relative stability of V_{min}) are due to a *decrease of* σ_{BG} *with increasing frequency* in terms of our model. Quantitatively, we can explain the experimentally observed increase of the hysteresis if we assume a suppression of the delocalization-related conductivity contribution from $\sigma_{BG}=1.3\times10^{-3}\sigma_{xy}$ at dc to $\sigma_{BG}=4.5\times10^{-4}\sigma_{xy}$ at $f=27$ Hz (for sample A). As the calculations show (see the Appendix), the observed frequency dependence of the hysteresis for sample A [Fig. 6(b)] means that the frequency dependence of σ_{BG} should demonstrate a strong drop at low frequencies from a dc value of $\sigma_{BG}(f=0)=1\times10^{-7}$ S, and then saturates at low values of about $(3-4)\times10^{-8}$ S (see Fig. 10 in the Appendix).

The essential parameter for σ_{BG} in the models discussed so far, taken into account, as a thermal, so as an electric field-related mechanism of electron delocalization,[11,16,17] is the localization length ξ (see the Appendix). An increase of the localization length yields an increase of the delocalization-related background conductivity in all theoretical models discussed so far concerning all regimes of delocalization-related transport in QH systems.[11,16,17] Consequently, the observed increase of the hysteresis with the frequency as reported above corresponds to a reduction of both

$\sigma_{\rm BG}$ and ξ with increasing frequency. The *strong drop of* $\sigma_{\rm BG}$ *at low frequencies means* a pronounced *reduction of the localization length*. In other words, the localization of electrons near local potential fluctuations becomes more effective already at low frequencies, as compared to the case of constant electric fields.

The very slow time scales of a hundreds of milliseconds or frequencies of around 10–20 Hz, on which we have observed so pronounced changes of the breakdown hysteresis curves, are not completely surprising. Such times appeared, for example, in the long tails of the far-infrared photoresponse of our structures,[18] where they can be attributed to the relaxation of the photoexcited electrons in the localization potential of samples. Even longer times (seconds and even hours) of the changes of the localization potential and corresponding changes of the delocalization-related transport were observed in direct experiments on investigations of the potential distributions in QH systems using single electron transistors on the top of the sample.[19–23] If one takes into account that these experiments were done at milliK temperatures, and our results were done at 1.5 K, one can see a reasonable explanation for the shorter relaxation times we observed. Also the earlier experiments (Refs. 20 and 21) pointed out the essential role of time-dependent delocalization for the transport in the QH regime.

VI. SUMMARY

To summarize, we have generated relaxation oscillations applying a quantum Hall Corbino device as a bistable switching element. The oscillation amplitude is determined by the dynamical hysteresis of the QH device. The frequency of the oscillation depends on the resistances and capacitances of the circuit, but also on the *dynamical* hysteresis of the Corbino device.

Our measurements of relaxation oscillations, supported by direct measurements of dynamical hysteresis in QH Corbino devices at different frequencies, revealed an increase of the hysteresis of the current-voltage curve in comparison with the value of the hysteresis at constant voltages. We have found that a dramatic increase of the breakdown hysteresis happens already at low (Hz-range) frequencies, and then this increase is caused mainly by an increase of the upper source-drain voltage limit of the hysteresis, $V_{\rm max}$. We explain the observed dynamical enhancement of the breakdown hysteresis by using an electron heating model and the assumption of a decreasing delocalization-related background component of the conductivity with increasing frequency. As the delocalization-related conductivity is a function of the electron localization length ξ in the existing models,[11,16,17] the observed increase of the hysteresis corresponds to a reduction of ξ with increasing frequency. Thus, our results indicate a dynamical reduction of the localization length in the quantum Hall Corbino systems near the breakdown of the QHE, when we increase the frequency accordingly from 0 Hz (dc) to 20–25 Hz.

ACKNOWLEDGMENTS

We would like to thank Professor R. J. Haug and Dr. F. Hohls for fruitful discussions, Dr. K. Eberl for providing the GaAs/ GaAlAs wafer. This study was supported by the Deutsche Forschungsgemeinschaft (DFG, Project No. Na235/10-2). B.E.S. acknowledges the support of the Deutscher Akademischer Austauschdienst (DAAD).

APPENDIX

The explanation for the existence of hysteresis of the current-voltage characteristics of QH devices at the breakdown of the quantum Hall effect can be derived from the electron heating model.[5,8] The hysteresis arises from the metastability of the power balance between gain (electrical energy fed to the system per time and area), $p_{\rm gain}=\sigma_{xx}E_r^2$ (σ_{xx} is the longitudinal conductivity of the QH system, E_r is the radial electric field in the Corbino device), and the energy loss rate $p_{\rm loss}=\varepsilon(T_{\rm el})\text{-}\varepsilon(T_L)/\tau_{\rm relax}$, which describes the relaxation of the enhanced energy $\varepsilon(T_{\rm el})$ at the elevated electron temperature $T_{\rm el}$ back to the energy $\varepsilon(T_L)$ at the lattice temperature T_L. The power balance equation between the gain and loss is written as

$$\sigma_{xx}(T_{\rm el})\cdot E_r^2=\frac{\varepsilon(T_{\rm el})-\varepsilon(T_L)}{\tau_{\rm relax}}=\frac{\Delta\varepsilon(T_{\rm el},T_L)}{\tau_{\rm relax}}, \quad \text{(A1)}$$

where $\tau_{\rm relax}$ is the corresponding relaxation time. The relaxation time depends on the electron temperature as $1/\tau_{\rm ep}=C_{\rm ep}T_{\rm el}^2$ ($C_{\rm ep}$ is an empirical parameter for inelastic electron-phonon scattering) for scattering at phonons.[8] Later investigations showed the dominance of scattering at impurities (which is related to the drift time τ_D between inelastic scattering events due to impurity-assisted inter-Landau-level tunneling) for the breakdown of the quantum Hall effect (Refs. 15 and 24),

$$\mathrm{T}_D=\ell_D/v_D=\ell_D BG(r_1,r_2)/V_{\rm SD}, \quad \text{(A2)}$$

with ℓ_D the inelastic scattering length, B the magnetic field, and $V_{\rm SD}$ the source-drain voltage, and with the geometry factor $G(r_1,r_2)$ for a Corbino ring (inner and outer boundary of the channel at the radii r_1 and r_2, maximum of E_r at r_1) with a homogeneous two-dimensional system:

$$G(r_1,r_2)=\ln\left(\frac{r_2}{r_1}\right)\cdot r_1, \quad \text{(A2a)}$$

such that the total scattering rate $1/\tau_{\rm relax}$ can be written as

$$\frac{1}{\tau_{\rm relax}}=\frac{1}{\tau_{\rm ep}}+\frac{1}{\tau_D}=C_{\rm ep}T_{\rm el}^2+\frac{V_{\rm SD}}{\ell_D BG(r_1,r_2)}. \quad \text{(A3)}$$

The energy of the electron system as a function of the temperature $\varepsilon(T)$ can be analytically calculated for the Fermi energy E_F situated in the middle of the Landau gap, if there is a constant background density of (localized) states $D_{\rm BG}$ and the relation $k_BT\ll\hbar\omega_c$ (k_BT: thermal energy, $\hbar\omega_c$: cyclotron energy) holds:

$$\varepsilon(T)=2\int_{E_F}^{\infty}(E-E_F)D(E)f(E,E_F,T)dE. \quad \text{(A4)}$$

($f(E,E_F,T)$ is the Fermi-Dirac distribution function), so that we obtain[15]

$$\Delta\varepsilon(T_{\rm el},T_L)=\frac{\pi^2 k_B^2}{6}D_{\rm BG}(T_{\rm el}^2-T_L^2). \quad \text{(A5)}$$

Introducing Eqs. (A3) and (A5) into the power balance equation, the relation between the radial electric field and the electron temperature can be evaluated, if the temperature dependence of the conductivity σ_{xx} is known:

$$\sigma_{xx}(T_{\rm el})=\sigma_0\exp\{-\Delta/k_BT_{\rm el}\}+\sigma_{\rm BG}. \quad \text{(A6)}$$

The first term in the sum of Eq. (A6) describes the thermal activation (the activation gap is $\Delta=\hbar\omega_c/2$), and the second term $\sigma_{\rm BG}$ is a background conductivity corresponding to delocalization-related tunnelling transport (also see Ref. 15). With this, the function $V_{\rm SD}(T_{\rm el})$ provides a direct access to the breakdown hysteresis:

$$V_{\rm SD}(T_{\rm el})=\frac{1}{2}V_{\rm Drift}+\sqrt{\frac{1}{4}V_{\rm Drift}^2+V_{\rm elph}^2}, \quad \text{(A7)}$$

with the drift contribution $V_{\rm Drift}(T_{\rm el})$

$$V_{\rm Drift}(T_{\rm el})=\frac{G(r_1,r_2)}{\ell_D B}\,\frac{\Delta\varepsilon(T_{\rm el},T_L)}{\sigma_{xx}(T_{\rm el})}, \quad \text{(A7a)}$$

and with the phonon scattering contribution $V_{\rm elph}(T_{\rm el})$

$$V_{\rm elph}(T_{\rm el})=G(r_1,r_2)\left[C_{\rm ep}T_{\rm el}^2\frac{\Delta\varepsilon(T_{\rm el},T_L)}{\sigma_{xx}(T_{\rm el})}\right]^{1/2}. \quad \text{(A7b)}$$

The electron temperature $T_{\rm el}$ as a function of the source-drain-voltage $V_{\rm SD}$, as obtained from inverting Eq. (A7), yields an S-shaped dependence. Since σ_{xx} is a monotonous function of $T_{\rm el}$ this corresponds to an S-shaped current-voltage ($I_{\rm SD}$-$V_{\rm SD}$) characteristics (Refs. 5 and 8). As the parts of the curves where $\partial T_{\rm el}/\partial V_{\rm SD}<0$ (and $\partial I_{\rm SD}/\partial V_{\rm SD}<0$, respectively) holds, are instable, a hysteresis in the corresponding experimental curves develops. The hysteresis is confined between two limiting values of $V_{\rm SD}$, $V_{\rm max}$, and $V_{\rm min}$ ($V_{\rm max}$ corresponds to lower and $V_{\rm min}$ to higher electron temperatures, $V_{\rm max}>V_{\rm min}$).

Both values, $V_{\rm max}$ and $V_{\rm min}$, depend on the parameters ℓ_D, B, $G(r_1,r_2)$, $D_{\rm BG}$, and $C_{\rm ep}$, and moreover essentially on the temperature dependence of $\sigma_{xx}(T_{\rm el})$. We calculate $\sigma_{xx}(T_{\rm el})$ according to Eq. (A6). The prefactor σ_0 was theoretically found equal $2e^2/h$ [where e is the elementary charge and h is the Planck constant (Ref. 9)], for long range scattering, confirmed by measurements of Svoboda *et al.* (Ref. 25).

The additional contribution to the resistivity, $\sigma_{\rm BG}$, is of crucial influence on the breakdown voltage $V_{\rm max}$. If a purely activated behavior of $\sigma_{xx}(T)$ is assumed, the electric power gain $\sigma_{xx}E_r^2$ is very small at low temperatures, even for rather large values of E_r. Thus the values of $V_{\rm max}$ become unrealistically high. To obtain values of $V_{\rm max}$ closer to the experiment, additional transport mechanisms leading to finite values of $\sigma_{\rm BG}$ have to be assumed.

We attribute $\sigma_{\rm BG}$ to delocalization-related tunneling transport, for which the different temperature dependences and parameters for $\sigma_{\rm BG}$ were proposed (Refs. 11, 16, and 17). (In our experimental situation, we have rather complicated electric-field-assisted and thermal-assisted tunneling (more correctly—the self-consistent mixture of both processes); therefore, it is most probably impossible to extract accurately characteristic parameters[11,16,17] of a certain model from our data.) However, the value of $V_{\rm min}$, which marks the lower limit of the hysteresis at higher electron temperatures, is nearly unaffected by the choice of $\sigma_{\rm BG}$. For the determination of $V_{\rm min}$, the activated conduction provides the dominating contribution.

To calculate the hysteresis, we used a value for electron-phonon scattering constant of $C_{\rm ep}=1.2\times10^7\ {\rm K}^{-2}\,{\rm s}^{-1}$ as reported in Ref. 8 for the filling factor $\nu=2$ and the activation energy $\Delta=\hbar\omega_c/2\propto B$. Applying these parameters, we found a better quantitative agreement of the calculations with the experimentally observed hysteresis with a geometry factor $G(r_1,r_2)$ of $r_2-r_1=200\ \mu$m instead of 110 μm as given by Eq. (A2a). This implies a better fit for a linear potential profile inside the 2D channel than for a $1/r$ profile, as expected for a Corbino device with a homogeneous conductivity tensor. Measurements of the potential profile inside a Corbino device by applying an atomic force microscope (Ref. 26) revealed a similar potential profile both in Hall bars and Corbino devices, including almost linear profiles at integer filling factors. Within this model, the variation of the parameters $D_{\rm BG}$, ℓ_D, and $\sigma_{\rm BG}$ affect the hysteresis limits $V_{\rm min}$ and $V_{\rm max}$ in a different ways:

(1) $V_{\rm min}$ and $V_{\rm max}$ increase with the density of states. For a sample with a mobility of about 10 m^2/V s, Stahl *et al.* (Ref. 27) reported a background density of states of $D_{\rm BG}=(5\pm1)\times10^9\ {\rm cm}^{-2}\,{\rm meV}^{-1}$. Figure 9(a) shows the hysteresis of the $T_{\rm el}$ vs $V_{\rm SD}$ curve for the corresponding range of $D_{\rm BG}$. The values for the scattering length and the background conductivity have been set to typical values [$\ell_D=10\ \mu$m, (see Ref. 12), and $\sigma_{\rm BG}=10^{-8}\ S=1.3\times10^{-4}\sigma_{xy}$ ($\nu=2$), (see Ref. 15)]. The best fit for the experimental value of $V_{\rm min}$ was obtained with $D_{\rm BG}=6\times10^9\ {\rm cm}^{-2}\,{\rm meV}^{-1}$, yielding a $V_{\rm min}$ just 10% below the measured value.

(2) $V_{\rm min}$ exhibits only a weak dependence on both ℓ_D and $\sigma_{\rm BG}$. This is due to the dominance of phonon-related scattering and activated transport at the higher electron temperatures, as relevant for $V_{\rm min}$. In turn, $V_{\rm max}$ depends distinctively on both parameters. As shown in Fig. 9(b), a strong increase of $V_{\rm max}$ is visible if ℓ_D is reduced from 50 to 5 μm. For impurity scattering lengths longer than 50 μm the dependence becomes weak due to the dominant contribution of the phonon-related scattering.

(3) With an increase of $\sigma_{\rm BG}$, $V_{\rm max}$ exhibits a pronounced decrease up to the complete disappearance of the hysteresis at $\sigma_{\rm BG}=1.3\times10^{-7}\ S=1.7\times10^{-3}\sigma_{xy}$ [Fig. 9(c)]. This is due to the dominance of the additional contribution of $\sigma_{\rm BG}$ (at $T_{\rm el}\approx6$ K at $V_{\rm max}$) to the conductivity at lower electron temperatures, at which the activated conductivity is negligible.

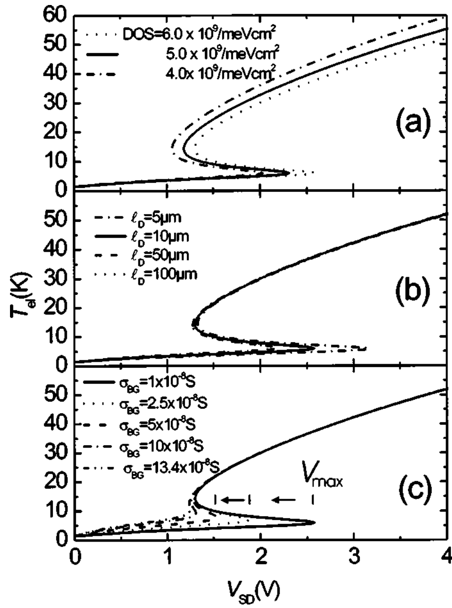

FIG. 9. The electron temperature T_{el} as a function of the source-drain voltage V_{SD}, for (a) different densities of states (DOS) for geometry parameters of sample A, $\mu = 100000\,\mathrm{cm}^2/\mathrm{V\,s}$, $l_D = 10\,\mu\mathrm{m}$, $\sigma_{\mathrm{BG}} = 10^{-8}\,\mathrm{S} = 1.3\times 10^{-4}\sigma_{xy}$ $(\nu = 2)$, $B = 5.7\,\mathrm{T}$, bath (lattice) temperature $T = 1.5\,\mathrm{K}$; (b) for different impurity scattering lengths l_D for the parameters of sample A, $D_{\mathrm{BG}} = 6\times 10^9\,\mathrm{cm}^{-2}\,\mathrm{meV}^{-1}$ (case #1, when as a result of the cooling cycle the resistance of the Corbino device in the resistive state was equal to $R_{\mathrm{CB}} = 76\,\mathrm{k}\Omega$); (c) for different values of σ_{BG}. σ_{xx} is a monotonous function of T_{el}, therefore the curves T_{el} (V_{SD}) yield a direct information about the hysteresis of $I-V$ characteristic of the Corbino device.

We have used the dependence of $V_{\max}$ on σ_{BG} to explain the observed increase of the dynamical hysteresis at low frequencies. In terms of our model, this increase is due to a decrease of σ_{BG}. In the models for for σ_{BG} discussed so far (see Refs. 11, 16, and 17), the essential parameter for σ_{BG} is the localization length ξ. An increase of the localization length yields an increase of the background conductivity irrespective of the mechanism, as thermally assisted, or as field-assisted delocalization. Consequently, the observed increase of the hysteresis with the frequency reported above corresponds to a reduction of both σ_{BG} and ξ.

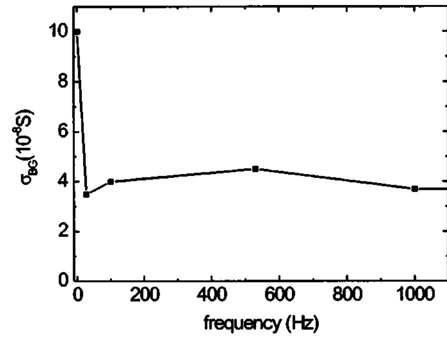

FIG. 10. Calculated values of the delocalization-related component of conductivity, at which we have the best fit of the electron heating model calculations with our experimentally determined frequency dependence of the hysteresis ΔV [Fig. 6(b)] for sample A.

The behavior of our frequency dependent hysteresis curves is qualitatively understandable in the frame of a delocalization-related picture: let us imagine that the electron in a static electric field is tunneling from one potential minimum to the other. There is a certain probability of this process, and a corresponding time of tunneling. Imagine, then, that we start to change the direction of the field with time into the opposite direction and back. What will happen when we increase this frequency of the change of the electric field direction? If our change is comparable to or quicker than the tunnelling time at this field amplitude, the electron simply will not tunnel. So, effectively, in the oscillating field we shall increase the electron localization and effectively suppress the transport, e.g., the conductivity of our system. Thus, in framework of such a delocalization-based model, we can readily expect a reduced localization length (more effective localization) with frequency.

Using the dependence of the hysteresis on the background conductivity as calculated, and the measured dynamical hysteresis as a function of the frequency, the frequency dependence of σ_{BG} can be deduced. A typical example is shown in Fig. 10. As expected, the delocalization-related conductivity (within the electron heating model as described above) shows a strong drop from a dc value of σ_{BG} $(f = 0) = 1\times 10^{-7}$ S at low frequencies, and then saturates at low values of about $(3-4)\times 10^{-8}$ S. In other words, the localization of electrons near local potential fluctuations becomes more effective at low frequencies, as compared to the case of constant electric fields.

*Present address: Department of Physics, Texas A&M University, College Station, Texas 77843-4242, USA.

[1] B. Van der Pol and J. Van der Mark, Nature (London) **120**, 363 (1927).
[2] E. R. Brown, J. R. Söderström, C. D. Parker, L. J. Mahoney, K. M. Molvar, and T. C. McGill, Appl. Phys. Lett. **58**, 2291 (1991).
[3] A. A. Andronov, A. A. Vitt, and S. E. Khaikin, *Theory of Oscillators* (Pergamon, Oxford, 1966).
[4] K. von Klitzing, G. Dorda, and M. Pepper, Phys. Rev. Lett. **45**, 494 (1980).
[5] G. Ebert, K. von Klitzing, K. Ploog, and G. Weimann, J. Phys. C **16**, 5441 (1983).
[6] M. E. Cage, R. F. Dziuba, B. F. Field, E. R. Williams, S. M. Girvin, A. C. Gossard, D. C. Tsui, and R. J. Wagner, Phys. Rev. Lett. **51**, 1374 (1983).
[7] G. Nachtwei, Physica E **4**, 79 (1999).
[8] S. Komiyama, T. Takamasu, S. Hiyamizu, and S. Sasa, Solid State Commun. **54**, 479 (1985); T. Takamasu, S. Komiyama, S. Hiyamizu, and S. Sasa, Surf. Sci. **170**, 202 (1986).
[9] D. G. Polyakov and B. I. Shklovskii, Phys. Rev. Lett. **74**, 150 (1995).
[10] F. Hohls, U. Zeitler, and R. J. Haug, Phys. Rev. Lett. **88**, 036802 (2002).
[11] M. Furlan, Phys. Rev. B **57**, 14 818 (1998).
[12] B. E. Sağol, G. Nachtwei, K. von Klitzing, G. Hein, and K. Eberl, Phys. Rev. B **66**, 075305 (2002).

[13] G. Nachtwei, N. G. Kalugin, B. E. Sağol, Ch. Stellmach, and G. Hein, Appl. Phys. Lett. **82**, 2068 (2003).
[14] W. F. Chow, *Principles of Tunnel Diode Circuits* (Wiley, New York, 1964).
[15] G. Nachtwei, Z. H. Liu, G. Lütjering, R. R. Gerhardts, D. Weiss, K. von Klitzing, and K. Eberl, Phys. Rev. B **57**, 9937 (1998).
[16] Y. Ono, J. Phys. Soc. Jpn. **51**, 237 (1982).
[17] D. G. Polyakov and B. I. Shklovskii, Phys. Rev. B **48**, 11 167 (1993).
[18] N. G. Kalugin, Yu. B. Vasilyev, S. D. Suchalkin, G. Nachtwei, B. E. Sagol, and K. Eberl, Phys. Rev. B **66**, 085308 (2002).
[19] J. Weis, Y. Y. Wei, and K. von Klitzing, Physica B **256–258**, 1 (1998).
[20] Y. Y. Wei, J. Weis, K. von Klitzing, and K. Eberl, Phys. Rev. Lett. **81**, 1674 (1998).
[21] Y. Y. Wei, Ph.D. dissertation, Max-Planck-Institut for Solid-State Physics, Stuttgart, 1998.
[22] J. Hüls, J. Weis, K. von Klitzing, and K. Eberl, Physica E **6**, 64 (2000).
[23] J. Hüls Ph.D. dissertation Fachbereich Physik der Universität Hamburg, 2001; and private communications.
[24] I. I. Kaya, G. Nachtwei, K. von Klitzing, and K. Eberl, Phys. Rev. B **58**, R7536 (1998).
[25] P. Svoboda, G. Nachtwei, C. Breitlow, S. Heide, and M. Cukr, Semicond. Sci. Technol. **12**, 264 (1997).
[26] E. Ahlswede, J. Weis, K. von Klitzing, and K. Eberl, Physica E **12**, 165 (2002); E. Ahlswede, Ph.D. thesis, Universität Stuttgart, 2002.
[27] E. Stahl, D. Weiss, G. Weimann, K. von Klitzing, and K. Ploog, J. Phys. C **18**, L738 (1985).